High resolution^{16}O(gamma^{*}, pi^{-}p) experiment

Aschenauer, E.C.; Castricum, H.L.; Cisbani, E.; de Bever, L.J.; Frullani, S.; Garibaldi, F.; Groep, D.L.; Iodice, M.; Kasdorp, W.J.; Lapikás, L.; Lee, F.X.; Onderwater, C.J.G.; Schroevers, M.; Spaltro, C.M.; Starink, R.

published in
Default journal
1998

document version
Publisher's PDF, also known as Version of record

High resolution $^{16}O(\gamma^*,\pi^-p)$ experiment

M. A. van Uden,[1] E. C. Aschenauer,[1] L. J. de Bever,[2] H. L. Castricum,[1] E. Cisbani,[3] S. Frullani,[3] F. Garibaldi,[3] D. L. Groep,[1] M. Iodice,[3] W-J. Kasdorp,[1] L. Lapikás,[1] F. X. Lee,[5] C. J. G. Onderwater,[1,4] M. Schroevers,[1] C. M. Spaltro,[1,4] R. Starink,[1,4] G. van der Steenhoven,[1] J. J. M. Steijger,[1] G. M. Urciuoli,[3] and L. E. Wright[6]

[1]*NIKHEF, P.O. Box 41882, 1009 DB Amsterdam, The Netherlands*

[2]*Department of Physics, University of Basel, CH-4056 Basel, Switzerland*

[3]*INFN Sezione Sanita' and Laboratorio di Fisica Istituto Superiore di Sanita', Viale Regina Elena 299, 00161 Rome, Italy*

[4]*Department of Physics and Astronomy, Free University, de Boelelaan 1081, 1081 HV Amsterdam, The Netherlands*

[5]*Department of Physics, University of Colorado, Boulder, Colorado 80309-0446*

[6]*Department of Physics, Ohio University, Athens, Ohio 45701*

(Received 11 June 1998)

The reaction $^{16}O(\gamma^*,\pi^-p)$ was studied with high energy resolution in the region of the Δ resonance at the AmPS facility of NIKHEF. Photoproduction cross sections were extracted for $1p_{1/2}$ and $1p_{3/2}$ neutrons in ^{16}O and the resulting pion and proton angular distributions are compared to model calculations by Lee, Wright, and Bennhold. The proton angular distributions are well described by the nonlocal version of the model and allow one to extract rms radii and spectroscopic factors for the $1p_{1/2}$ and $1p_{3/2}$ neutron shells. The same calculations are in fair agreement with the pion angular distributions.
[S0556-2813(98)05812-9]

PACS number(s): 25.20.−x, 21.60.−n, 27.20.+n

I. INTRODUCTION

Many experiments and theoretical calculations in subatomic physics have yielded a good understanding of the nucleon-nucleon interaction. However, the interaction between a nucleon and the Δ, which is a $S=\frac{3}{2}$, $T=\frac{3}{2}$ baryon resonance at an invariant mass of 1232 MeV, is less well known. Studies of the nucleon-Δ interaction are rather difficult because the Δ is not a stable particle. The best way to study it experimentally is by comparing Δ production on a nucleon to Δ production in a nucleus, and observe the subsequent decay into a pion and a nucleon.

In the past pion-induced Δ production on the free nucleon has been extensively studied, followed by experiments on selected nuclei [1]. However, pion scattering experiments mainly probe the surface region of the nucleus. In order to study the high density region inside the nucleus (virtual) photons of a few hundred MeV should be used, thus avoiding the strong initial state interactions of the incoming pions.

Lee, Wright, and Bennhold have developed a model describing the elementary process of photoproduction of a pion and a proton on a nucleus in the region of the Δ resonance [2]. By comparing their model to previous experiments they have shown that at backward pion angles the production and propagation of the Δ in a nucleus can be treated adequately in the distorted wave impulse approximation (DWIA). However, at backward angles with respect to the incoming photon the photoproduction cross section exhibits little sensitivity to Δ propagation effects, whereas an enhanced sensitivity is expected at forward pion angles. Hence, a systematic study of possible medium effects requires the comparison of experimental results in both kinematic regimes with calculations using the same quasifree approach. Possible effects of the nuclear medium can be mimicked in the calculations by changing the mass or width of the Δ, or by a change in the $E2/M1$ ratio describing the excitation of the Δ. Previous experiments were unable to draw solid conclusions on this topic, because they did not probe the kinematic region where the Δ contribution is largest (at forward pion angles) or because of low statistics.

In this paper new experimental results are presented for electroproduction of π^-p pairs on ^{16}O in the region of the Δ resonance. Photoproduction cross sections for the reaction $^{16}O(\gamma,\pi^-p)$ were extracted using virtual photon theory. The experiment was carried out with the AmPS facility at NIKHEF. We measured both the proton angular distribution, which gives information on the reaction mechanism and probes the neutron wave functions in ^{16}O, and the pion angular distribution, which is aimed at studying Δ-propagation effects inside the nucleus. The high resolution instrumentation developed for this experiment has been described in detail elsewhere [3]. In this paper the subject is introduced by providing an outline of the theoretical framework that is used for the description of the (γ,π^-p) reaction (Sec. II) and a review of earlier experiments (Sec. III). In Sec. IV we describe the present experiment and in Sec. V a comparison of the measured angular distributions to calculations in the model of Lee, Wright, and Bennhold is given. Section VI concludes the paper.

II. THEORETICAL FRAMEWORK

The propagation and possible modification of the Δ resonance in a nucleus involve the excitation of a Δ using—in our case—an incident virtual photon beam. As the lifetime of the Δ is too short to detect it directly (10^{-23} s; i.e., it will propagate on average 3 fm before it decays), two decay products are detected instead. In the present experiment the decay channel of the Δ, leading to a negatively charged pion and a proton, is examined by detecting a pion and a proton in coincidence.

A. Kinematics

In a relativistic description of the photoproduction reaction $(\gamma,\pi^- p)$ energy and momentum conservation requires that

$$E_\gamma = T_p + (T_\pi + m_\pi) + T_{^{15}O} + E_x + Q, \tag{1}$$

$$\vec{p}_\gamma = \vec{p}_p + \vec{p}_\pi + \vec{p}_{^{15}O}, \tag{2}$$

where the quantities T, $\vec{p}$, and $m(M)$ denote the kinetic energies, momenta, and rest masses of the proton (p), the pion (π), and the recoil nucleus (^{15}O), respectively. The quantity E_x denotes the excitation energy of the recoil nucleus and the Q value is defined as $M_{^{15}O} + m_p - M_{^{16}O}$, which is closely related to the binding energy E_b of the neutron in ^{16}O, i.e., $E_b = Q + m_n - m_p \approx Q$. In these equations E_γ is the energy of the photon and $\vec{p}_\gamma$ its momentum vector $(E_\gamma = |\vec{p}_\gamma|)$.

The relevant kinematic observables of the reaction are the missing energy E_m, which is defined as

$$E_m = E_\gamma - T_p - (T_\pi + m_\pi) - T_{^{15}O}, \tag{3}$$

and the missing momentum p_m, which is defined as the negative of the recoil momentum:

$$\vec{p}_m = \vec{p}_p + \vec{p}_\pi - \vec{p}_\gamma = -\vec{p}_{^{15}O}. \tag{4}$$

In the present experiment we are mainly interested in transitions leading to the ground state and first strongly excited state of ^{15}O. The ground state transition corresponds to $\pi^- p$ photoproduction on a neutron in the $1p_{1/2}$ shell. In this case the missing energy E_m will be equal to the Q value of the reaction (14.365 MeV). The transition to the first strongly excited state at 6.176 MeV corresponds to $\pi^- p$ photoproduction on a neutron in the $1p_{3/2}$ shell and results in $E_m = 20.541$ MeV. The central kinematics for the reaction was set such that both transitions were covered by the experimental energy acceptance. Excitation of the non-natural parity doublet at 5.2 MeV in ^{15}O is expected to be negligibly small within the present experimental accuracy since the spectroscopic factors for the isobaric analog transitions in the reaction $^{16}O(e,e'p)^{15}N$ are a factor of 20 smaller [10] than that for the strong $1p_{3/2}$ transition.

B. $(\gamma,\pi^- p)$ cross section

For a description of the cross section often the factorized DWIA formalism is used, as first developed for the $(\gamma,\pi^- p)$ reaction by Laget [4]. In this formalism the cross section is written as [5]

$$\frac{d^5\sigma}{dT_\pi d\Omega_\pi d\Omega_p} = k\sigma^{\text{c.m.}}_{\gamma n\to\pi p}|\Phi_l^D|^2, \tag{5}$$

in which k is a kinematic constant including a recoil term, $\sigma^{\text{c.m.}}_{\gamma n\to\pi p}$ the elementary Δ-production cross section on a free neutron in the center-of-mass framework, and Φ_l^D the distorted momentum distribution of the neutron:

$$\Phi_l^D = \int \chi_{\pi^-}^{-(*)}\chi_p^{-(*)} e^{i\vec{k}_\gamma\cdot\vec{r}}\phi_l(\vec{r})d\vec{r}. \tag{6}$$

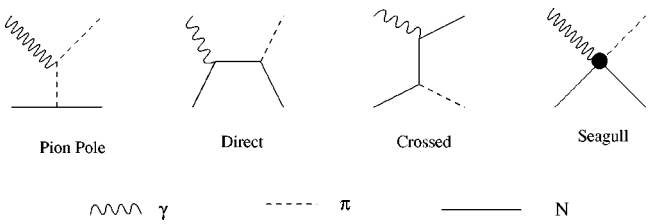

FIG. 1. Born terms in the pion production amplitude.

In this equation $\chi^{-(*)}$ is the distorted wave of the outgoing proton or pion and ϕ_l the wave function of the neutron, with orbital momentum quantum number l.

The Δ-production cross section $\sigma^{\text{c.m.}}_{\gamma n\to\pi p}$ includes, apart from processes in which a Δ is excited, also processes where a pion and a proton emerge from the nucleus without an intermediate Δ being produced, the ''Born terms'' (see Fig. 1). The seagull term is required to maintain gauge invariance when pseudovector coupling is used at the $NN\pi$ vertex.

The relative contribution of the Δ term and the Born terms depends on the chosen kinematics. Especially the pion angle with respect to the incoming photon is important. While at backward pion angles the Born terms dominate, the Δ and Born terms are of equal size at forward pion angles. This is demonstrated in Fig. 2. Therefore, possible modifications of the Δ in the nucleus are best studied at forward pion angles.

The factorized approach [i.e., Eq. (5)] is based on the assumption that the Δ-production mechanism and the final-state interaction are decoupled. In general this assumption cannot be justified *a priori*, and the Δ-production operator should be included in the integral of Eq. (6). For this reason more recent DWIA calculations are not based on the factorization ansatz anymore. Our data are compared to such a calculation, i.e., the work of Lee, Wright, and Bennhold [2]. The ingredients of this calculation can be identified using the quantities defined in Eqs. (5) and (6).

(i) The full Blomqvist-Laget pion photoproduction operator [6,7] was used [analogous to $\sigma^{\text{c.m.}}_{\gamma n\to\pi p}$ in Eq. (5)].

(ii) The pion optical potential of Carr, McManus, and Stricker [8] was used for the evaluation of the pion distorted wave function, i.e., $\chi^-_{\pi^-}$ in Eq. (6).

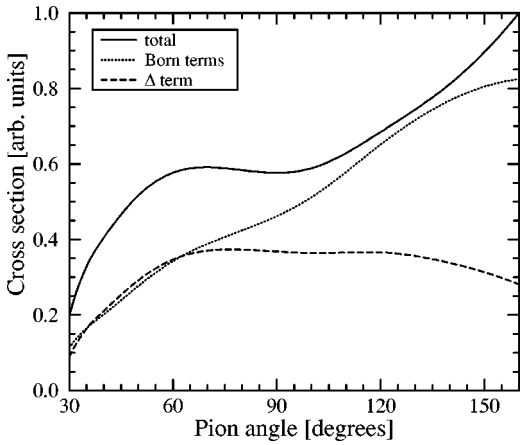

FIG. 2. Total cross section and the relative contributions of the Born and Δ terms as a function of the pion angle, evaluated in a factorized DWIA calculation using a modified version of the code THREEDEE [5].

(iii) The global phenomenological optical potential of Schwandt *et al.* [9] was used for the evaluation of the proton distorted wave function χ_p^- in Eq. (6).

(iv) Harmonic oscillator wave functions were used for the bound-state wave function ϕ_l. The normalization of ϕ_l was chosen so as to correspond to the observed reduction of proton spectroscopic factors found in the reaction $^{16}\mathrm{O}(e,e'p)$ [10]. It is assumed that *NN* correlations cause a similar reduction of spectroscopic factors compared to independent-particle shell-model (IPSM) values for neutrons as for protons.

In the calculation possible medium modifications are neglected, and only free production amplitudes are used. The cross sections for the reaction (γ,π^-p) were computed in both the local and nonlocal formalisms [2]. In the nonlocal model the momenta of the various particles enter the Blomqvist-Laget photoproduction operator, resulting in a six-dimensional integral in momentum space. In the local model the photoproduction operator is approximated by a *local* form that does not depend on the momenta of the various particles, but only on their relative coordinates, resulting in a conventional three-dimensional integral in r space.

In the past, Δ-hole model calculations were used to describe pion-production experiments. The Δ-hole model treats the Δ excitation as the dominant process in the reaction. In the propagator of the Δ (and its associated hole) medium effects can be introduced. This model was first applied to photoabsorption reactions by Koch, Moniz, and Ohtsuka [11], and recent applications to the (γ,π^-p) reaction were published by Sato and Takaki [12]. These calculations showed that the Δ-hole effects are rather small for the (γ,π^-p) reaction at 360 MeV. For that reason calculations in the Δ-hole model were not considered for the interpretation of the present data.

III. PREVIOUS EXPERIMENTS

Two experiments similar to the one presented in this paper were performed in the past. The first experiment studied the reaction $^{12}\mathrm{C}(\gamma,\pi^-p)$ at the Tomsk synchrotron [13]. In this experiment the photon energy was 380 MeV, and the experiment was limited to one angular setting. The pion angle was fixed at a backward angle of 120° and the proton angle at 20°. The large range of proton energies that were included in the acceptance enabled the extraction of the cross sections for removal of both p- and s-shell neutrons. The two p states could not be separated because of a lack of energy resolution.

Comparison of the Tomsk data to calculations in the local DWIA framework presented above showed a reasonable agreement, while the full nonlocal calculation describes the data even better (see Ref. [2]). As the cross section at backward pion angles is largely driven by Born terms, it is concluded that both the Born terms and the final-state interaction are well treated in the DWIA approach.

The second experiment was performed at MIT Bates [14]. Here the out-of-plane cross section distribution was measured at pion angles of 64° and 120°, such that a possible modification of the Δ-production and propagation mechanism might be observed. The proton detector, placed under 40° and 20°, respectively, consisted of five ΔE-E scintillators, which were placed in a vertical array covering out-of-plane angles from $-22°$ to $+22°$ with respect to the photon-pion scattering plane. Low pion-proton coincidence counting rates made it necessary to integrate over a wide range of pion energies. This makes comparison to other exclusive (γ,π^-p) experiments rather difficult and calculations rather laborious. Calculations in the best (nonlocal) framework were therefore not performed.

At the backward pion angle of 120° the local calculation of the cross section shows a fair agreement with the data (see Ref. [2]). At the forward pion angle no agreement between the data and the calculation is found, as the calculation overestimates the data by about a factor of 4. An *ad hoc* reduction of the in-medium Δ mass by 5% brings the calculation much closer to the data [2]. Such a modification of the Δ mass can be employed to include some Δ-medium effects in a purely phenomenological way, but it does not have a physical meaning by itself. One of the key issues to be addressed in the present experiment is the verification (or falsification) of this observation, especially in view of the large systematic (30%) and statistical (50%) uncertainties of the MIT experiment. In this respect one has to realize that a (γ,π^-p) coincidence experiment at a low duty factor beam, using a nonmagnetic detector (as used at MIT), is at the edge of possibilities in view of the high single count rates involved.

IV. EXPERIMENTAL TECHNIQUE

The experiment was performed in the EMIN experimental area at NIKHEF. An almost continuous electron beam was created by injecting 369 MeV electrons from the linear electron accelerator MEA into the pulse stretcher ring AmPS [15], which were subsequently extracted and guided to the target. The resulting average electron current was 7 μA, the macroscopic duty factor about 70%.

Instead of using a tagger magnet in order to create a pure real photon beam, the target was exposed to an electron beam. In such a case, both real and virtual photons are created in the target itself. Tiator and Wright [16] have described a formalism to extract photoproduction cross sections from such electroproduction data using virtual photon theory. A correction (of 4.7%) has been applied for the amount of real photons contributing to the cross section (see Ref. [17]). The corresponding number of virtual photons in the top 10 MeV is 3×10^{12} photons/s at a beam energy of 369 MeV and a current of 7 μA. This number is more than four orders of magnitude larger than available at a typical photon-tagging facility. Because the shape of the virtual photon spectrum is well known, the (γ,π^-p) cross sections can be extracted accurately from end-point fits to the measured yield (see Fig. 3). The cross section shown results from a standard coincidence data analysis [3] that includes subtraction of accidental coincidences and weighting by the detection volume.

The particles emerging from the target were detected with the high-resolution two-spectrometer setup in the EMIN hall [18]. Protons were detected in the QDD spectrometer. Pions were detected in the QDQ spectrometer, which was equipped with an aerogel Čerenkov detector in order to discriminate between pions and protons [3]. A correction was made for decay of pions on their way from target to detector. Given

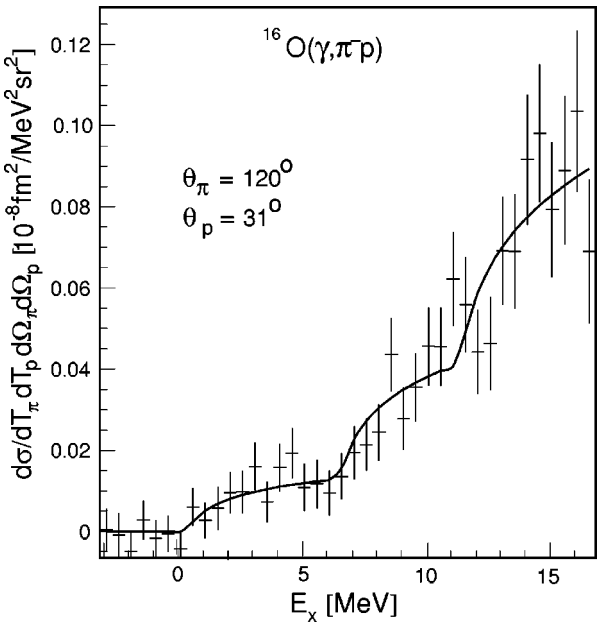

FIG. 3. Sixfold differential cross section as a function of the excitation energy, measured at $\theta_\pi = 120.0°$ and $\theta_p = 31.1°$. The solid curve represents the end-point fit to the data.

the known flight path length of 7.64 m the fraction of pions that reached the detector was calculated to range from 0.47 to 0.59, depending on pion momentum.

We used ^{16}O as a target nucleus since its double closed-shell structure facilitates the interpretation of the results, as the wave functions are generally well known. A triple-foil waterfall target was employed, which is described in more detail in Refs. [3] and [19]. Making use of the well-known magnetic properties of the spectrometers [18], it was possible to accurately determine the vertex point and thus to separate events that have occurred in the first, middle, or last foil. Using an energy-loss calculation for each foil separately we achieved an overall missing-energy resolution of about 0.5 MeV. This allowed us to extract values for the cross section of individual states in the residual nucleus ^{15}O.

The target thickness was calibrated by measuring the cross section for elastic electron scattering on oxygen at a scattered electron angle of 60°. This angle was chosen because the angular dependence of the cross section is almost flat in this region, resulting in a small error in the determination of the target thickness. The measurement resulted in a target thickness of 205 mg/cm^2. The statistical error associated with this value is rather small (1%). The major contribution to the systematic error is the uncertainty in the existing elastic electron-scattering cross-section data, which is about 3% [10]. The total systematic error in the $(\gamma,\pi^- p)$ cross sections is 6%.

TABLE I. Central kinematics for the pion angular distribution measurements.

Kinematics	θ_π [°]	T_π [MeV]	θ_p [°]	T_p [MeV]
$\theta_\pi = 40°$	40.00	155.0	54.32	55.1
$\theta_\pi = 60°$	60.00	140.0	55.02	70.1
$\theta_\pi = 80°$	80.00	125.0	47.94	85.1
$\theta_\pi = 100°$	100.00	110.0	39.37	100.1
$\theta_\pi = 120°$	120.00	95.0	31.10	115.1
$\theta_\pi = 135°$	135.00	87.5	25.93	122.6

TABLE II. Central kinematics for the proton angular distribution measurements.

Kinematics	θ_π [°]	T_π [MeV]	θ_p [°]	T_p [MeV]
$p_m = 57$ MeV/c	120.00	95.0	25.93	115.3
$p_m = 100$ MeV/c	120.00	95.0	31.10	115.1
$p_m = 150$ MeV/c	120.00	95.0	37.09	114.6
$p_m = 200$ MeV/c	120.00	95.0	43.14	114.0
$p_m = 250$ MeV/c	120.00	95.0	49.28	113.2

The final cross sections $d^5\sigma/d\Omega_\pi d\Omega_p dE_\pi$ were deduced from end-point fits to the spectra, as exemplified in Fig. 3, using the relation

$$\frac{d^6\sigma}{d\Omega_\pi d\Omega_p dE_\pi dE_m} = \frac{N_\gamma(E_e,E_\gamma)}{E_\gamma}\,\frac{d^5\sigma}{d\Omega_\pi d\Omega_p dE_\pi}\,\frac{dE_\gamma}{dE_m}. \tag{7}$$

Here the quantity $N_\gamma(E_e,E_\gamma)$ represents the Dalitz-Yennie distribution of virtual photons [16], simplified for infinitely massive recoil [17], and dE_γ/dE_m is a recoil factor resulting from the integration over missing energy. The uncertainty involved in using the Dalitz-Yennie shape of the virtual photon spectrum instead of the recoil-corrected Tiator-Wright shape is largest for the $\theta_\pi = 135°$ measurement (about 1%). Near the end point the difference is somewhat larger (about 5%), but as the dominant statistical weight comes from the region between 2 and 5 MeV, where the uncertainty is 1% or less, the overall systematic uncertainty related to the chosen shape of the virtual photon spectrum is only 1%.

The kinematic settings of the experiment are presented in Tables I and II, the measured cross sections in Tables III and IV. Note that the data point at $\theta_\pi = 120°$ and $p_m = 100$ MeV/c appears in both sets of tables.

The experiment consisted of two parts. A proton angular distribution was measured with a fixed backward pion angle of 120°, a kinematic domain where the cross section is well described in the model of Lee, Wright, and Bennhold, but with little sensitivity to the Δ contribution. These data serve to verify with higher precision than before whether the quasifree Δ-production formalism can properly describe the $(\gamma,\pi^- p)$ cross section. Moreover, the precision of the present experiment enabled us to extract information on the

TABLE III. Cross sections $d^5\sigma/d\Omega_\pi d\Omega_p dE_\pi$ [μb/MeV sr^2] as a function of θ_π at an electron beam energy of 369.1 MeV and $p_m = 100$ MeV/c. The indicated errors are statistical only.

θ_π [°]	$\sigma_{p_{1/2}}$	$\sigma_{p_{3/2}}$
40	0.160±0.032	0.206±0.059
60	0.135±0.016	0.239±0.043
80	0.147±0.016	0.284±0.049
100	0.100±0.018	0.322±0.051
120	0.126±0.019	0.276±0.049
135	0.167±0.025	0.413±0.049

TABLE IV. Cross sections $d^5\sigma/d\Omega_\pi d\Omega_p dE_\pi$ [μb/MeV sr^2] as a function of θ_p at an electron beam energy of 369.1 MeV and $\theta_\pi = 120°$. The indicated errors are statistical only.

θ_p [°]	p_m [MeV/c]	$\sigma_{p_{1/2}}$	$\sigma_{p_{3/2}}$
25.93	57	0.053±0.014	0.201±0.037
31.10	100	0.126±0.019	0.276±0.049
37.09	150	0.077±0.013	0.229±0.034
43.14	200	0.024±0.009	0.114±0.024
49.28	250	0.010±0.007	0.022±0.015

neutron bound-state wave functions from these data. Hence, the hitherto unexplored spectroscopic strength for $1p$ neutrons in ^{16}O can be determined. In the second part of the experiment a pion angular distribution was measured at a fixed missing momentum of 100 MeV/c. The measured kinematic domain also included the forward pion angles, where the cross section is increasingly sensitive to the contribution of the Δ, thus yielding information about possible medium modifications of the Δ. The missing momentum was fixed at 100 MeV/c by varying both the pion angle (in large steps) and the proton angle (in relatively small steps).

V. RESULTS

A. Proton angular distributions

In Figs. 4 and 5 the data for the proton angular distribution for the ground state and first excited state, respectively, are shown together with plane wave impulse approximation (PWIA), local DWIA, and nonlocal DWIA calculations. The harmonic oscillator range parameter used in the calculations is $b = 1.81$ fm, corresponding to a rms radius of the neutron $1p$ wave function of 2.86 fm. Spectroscopic factors S_α of 1.2 and 2.4 have been applied for the ground state and first excited state, respectively. The nonlocal DWIA calculations are in good agreement with the data, confirming the validity of the quasifree DWIA framework at a pion angle of 120°. The difference between the local and nonlocal DWIA curves shows the importance of accounting for nonlocal effects in the $(\gamma,\pi^- p)$ reaction. From the difference between the PWIA and DWIA curves it is deduced that the final-state interaction reduces the cross section by a factor of 2 in these kinematics.

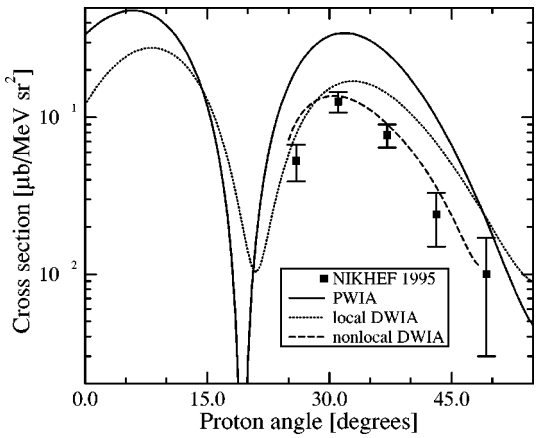

FIG. 4. Cross section for the proton angular distribution of the reaction ^{16}O$(\gamma,\pi^- p)$ at $\theta_\pi = 120°$, leading to the ground state in ^{15}O. The curves represent calculations with a rms radius of 2.86 fm for the neutron wave function and $S_\alpha = 1.2$.

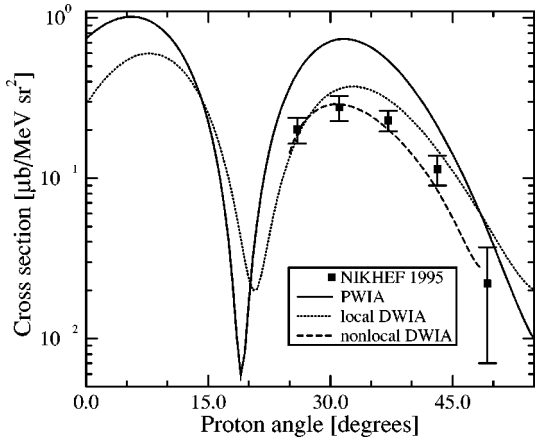

FIG. 5. As in Fig. 4, but for the 6.176 MeV state and $S_\alpha = 2.4$.

An improved description of the data was obtained by fitting the spectroscopic factor and the radius of the bound-state wave function. The results of this fit are displayed in Figs. 6 and 7. For both the $1p_{1/2}$ shell and the $1p_{3/2}$ shell a good description of the data is obtained. The numerical results for the rms radii of the neutrons and the corresponding spectroscopic factors are shown in Table V, where they are compared to the rms radii and spectroscopic factors for $1p$ protons in ^{16}O derived from high resolution ^{16}O$(e,e'p)$ data [10]. The errors listed in Table V for the proton results represent the full range of possible values for the rms radii and spectroscopic factors that was obtained by using different potentials to describe the final-state interaction. The errors for the $(\gamma,\pi^- p)$ results are statistical only. Thus far no systematic study of the uncertainty related to the optical potentials used in the $(\gamma,\pi^- p)$ calculation has been performed.

The rms radii of the neutron wave functions extracted from the $(\gamma,\pi^- p)$ data using the nonlocal DWIA formalism are in good agreement with the values for the proton wave functions. The local DWIA values are about 15% higher than the proton values.

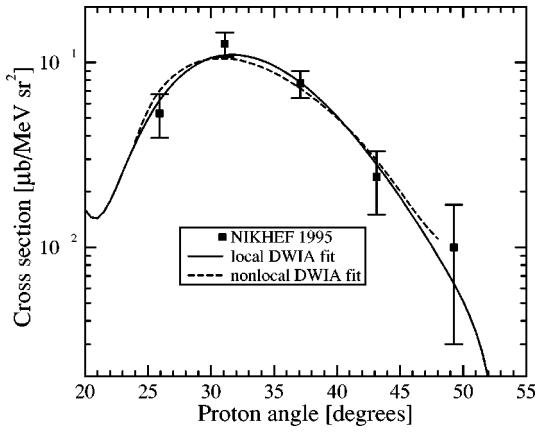

FIG. 6. Cross sections for the proton angular distribution of the reaction ^{16}O$(\gamma,\pi^- p)$, leading to the ground state in ^{15}O. The curves are fitted to the data, with the rms radius of the neutron bound-state wave function and the spectroscopic factor treated as free parameters.

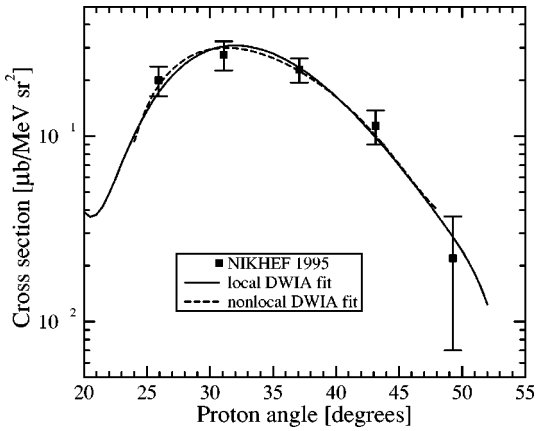

FIG. 7. As in Fig. 6, but for the 6.176 MeV state.

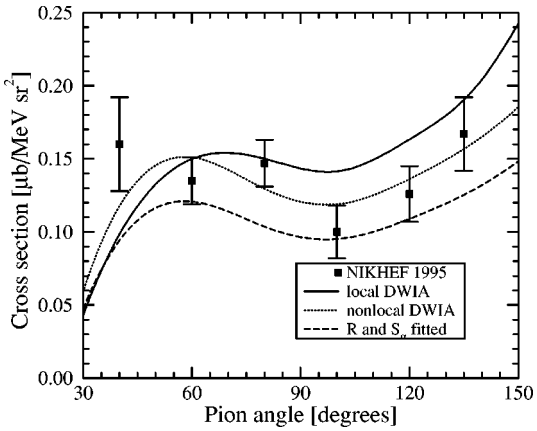

FIG. 8. Cross section for the pion angular distribution of the reaction $^{16}O(\gamma,\pi^- p)$, leading to the ground state in ^{15}O. The solid and dotted curves are evaluated using an rms radius of 2.86 fm and a spectroscopic factor of 1.2, while the dashed curve was evaluated using the values displayed in Table V.

The neutron spectroscopic factors derived from the $(\gamma,\pi^- p)$ data are consistent with those derived for the proton from the reaction $(e,e'p)$. The value for the $1p_{1/2}$ neutron shell is somewhat low but not inconsistent with the corresponding proton result. It should be noted that the value quoted for the $1p_{3/2}$ shell includes all $1p_{3/2}$ strength between excitation energies from 6 to 11 MeV. The $1p_{3/2}$ proton strength is known to be fragmented (see Ref. [10]) in this domain, but as all this strength is effectively included in the $(\gamma,\pi^- p)$ end-point fit, the contribution of all states observed in this domain in the reaction $(e,e'p)$ has to be summed for a proper comparison. The spectroscopic factors evaluated using the local DWIA calculation are significantly below the proton values, showing once more the importance of nonlocality effects in the reaction $(\gamma,\pi^- p)$.

The present results for the spectroscopic strengths of neutrons in a complex nucleus are the first ones obtained via an electromagnetically induced reaction. Such results can also be obtained with the quasifree reaction $(e,e'n)$. However, this type of experiment is much more laborious to perform because of the difficulty to achieve the required high resolution and to detect neutral particles in a hostile electron beam environment. In the present experiment this difficulty was circumvented by detecting charged particles in high resolution magnetic spectrometers. Obviously, the reaction mechanism for the reaction $(\gamma,\pi^- p)$ is less well known than that of the reaction $(e,e'n)$, but the good description of our experimental cross sections lends support to the conclusion that the deduced neutron spectroscopic factors are accurate to within 20%. The established values demonstrate for the first time that the observed [10] large depletion of proton valence shells in ^{16}O (which was also observed for a large number of other nuclei [20]) is also present for the neutron valence shells in ^{16}O. This confirms the explanation for such a depletion that was given [21] in terms of long- and short-range correlations, which are expected to affect both neutron and proton wave functions in a similar way.

TABLE V. Fit values of rms radius and spectroscopic factor for the $1p_{1/2}$ and $1p_{3/2}$ neutron shells in ^{16}O, determined from the present $^{16}O(\gamma,\pi^- p)$ data. The corresponding proton results derived from $(e,e'p)$ data [10] are also listed. The errors in the $(e,e'p)$ results include model uncertainties, while the errors in the $(\gamma,\pi^- p)$ results are statistical only.

	rms radius [fm]		
	$(e,e'p)$	$(\gamma,\pi^- p)$	
		Nonlocal	Local
$1p_{1/2}$	2.90±0.07	2.86±0.17	3.40±0.33
$1p_{3/2}$	2.74±0.06	2.80±0.13	3.14±0.19
	S_α		
	$(e,e'p)$	$(\gamma,\pi^- p)$	
		Nonlocal	Local
$1p_{1/2}$	1.25±0.03	0.96±0.19	0.49±0.11
$1p_{3/2}$	2.65±0.22	2.81±0.43	1.56±0.24

B. Pion angular distributions

In Figs. 8 and 9 the results for the pion angular distribution are displayed. The nonlocal and local DWIA calculations have been evaluated using a neutron rms radius of 2.86 fm and spectroscopic factors of 1.2 and 2.4 for the $1p_{1/2}$ and $1p_{3/2}$ states, respectively. Also shown is a nonlocal calculation using the rms radii and spectroscopic factors extracted from the proton angular distribution, as listed in Table V. It should be noted that the dashed curves in Figs. 8 and 9 are uncertain by 20% due to the errors quoted in Table V.

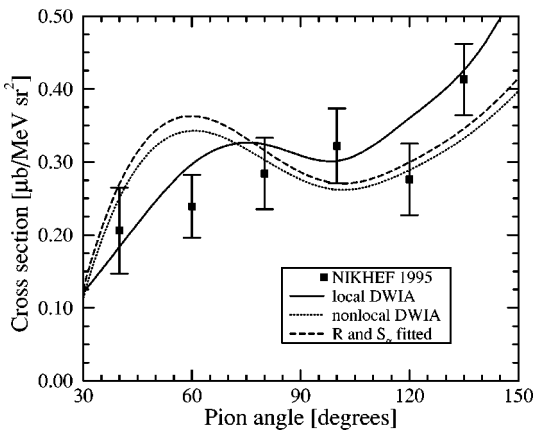

FIG. 9. Same as in Fig. 8 but for the 6.176 MeV state.

At backward pion angles the calculations are in good agreement with the data for both states. This confirms the expectation that at backward pion angles—where the Born terms dominate over the Δ term—the cross section can be well described using a quasifree reaction mechanism.

For the $1p_{1/2}$ shell all calculations essentially agree with the data. The curve based on the fitted S_α value is somewhat low, but still consistent with the data, if the aforementioned 20% uncertainty is considered.

For the $1p_{3/2}$ shell the nonlocal calculations overestimate the data at forward pion angles. In fact, the calculation based on the experimentally determined rms radius and spectroscopic factor overestimates the $1p_{3/2}$ data by 50% for $\theta_\pi = 60°$. In this domain similar calculations overestimated the MIT data by a factor of 4. On the other hand, a recent $^{12}C(\gamma,\pi^+ n)$ experiment [22] did not reveal any discrepancy between DWIA calculations and the data. This experiment was performed at Mainz with real photons at incident photon energies close to the ones of the present experiment. However, the energy resolution of the Mainz experiment (8 MeV) and the photon energy binning (40 MeV) may have washed out any discrepancy. Moreover, the data were not compared to the same type of nonlocal DWIA calculations as used here.

The seemingly different behavior of the $1p_{1/2}$ and $1p_{3/2}$ transitions is difficult to understand because most ingredients of the DWIA $(\gamma,\pi^- p)$ calculations are not—or only mildly—spin dependent. Moreover, an explanation in terms of a medium modification of the Δ is unlikely, as there are no calculations predicting a large influence of medium effects on the $1p_{3/2}$ shell that are absent on the $1p_{1/2}$ shell. On the other hand, in Ref. [2] it was shown that the $E2/M1$ ratio influences the pion angular distribution. The $E2/M1$ ratio represents the contribution from the transverse quadrupole component of the Δ, which gives rise to a small d-state component. This ratio ranges from 0 to -5 % depending on the theoretical approach involved. A variation of the $E2$ contribution within this range has only little influence on the cross section [2]. This influence is peaked around a pion angle of 80° and is also large at backward pion angles ($\geqslant 120°$). A reduction of the $E2/M1$ ratio enhances the cross section around 80° and reduces it at backward pion angles, and vice versa. Hence, in order to explain the different behavior of the pion angular distributions the $E2/M1$ ratio must be different for the two transitions: the $p_{1/2}$ distribution should favor a larger $E2/M1$ ratio and the $p_{3/2}$ a smaller one. We do not know any calculations that predict such an effect.

VI. CONCLUSIONS

We have presented the results of a high resolution $\pi^- p$ electroproduction experiment on ^{16}O in which it was possible to separate the ground state and first excited state in ^{15}O. From the data photoproduction cross sections were deduced as a function of both proton and pion angle.

The proton angular distributions are well reproduced by DWIA calculations, thus confirming the quasifree nature of the $(\gamma,\pi^- p)$ reaction in the present kinematic domain. The results demonstrate that the $(\gamma,\pi^- p)$ reaction at backward pion angles is well understood and can be used to study the dynamics of neutrons in complex nuclei. The data have been used to determine the rms radius and spectroscopic factors of the $1p_{1/2}$ and $1p_{3/2}$ neutron wave functions in ^{16}O. The results are in remarkable agreement with those derived from $^{16}O(e,e'p)$ data for the corresponding proton orbitals [10]. Therefore, they further corroborate the explanation given for the large depletion of valence nucleon shells in terms of long- and short-range correlations [21].

At backward angles the measured pion angular distributions and calculations are in fair agreement. At forward pion angles they revealed a slightly different behavior for the $1p_{1/2}$ and $1p_{3/2}$ shells, which was not expected. However, it has been argued that it is unlikely that this difference is related to modifications of the Δ inside a nucleus.

This work was part of the research program of the Foundation for Fundamental Research of Matter (FOM), which is financially supported by the Netherlands Organization for Advancement of Pure Research (NWO).

[1] G. S. Kyle *et al.*, Phys. Rev. Lett. **52**, 974 (1984).
[2] F. X. Lee, L. E. Wright, and C. Bennhold, Phys. Rev. C **48**, 816 (1993).
[3] G. van der Steenhoven *et al.*, Nucl. Instrum. Methods Phys. Res. A **399**, 160 (1997); M. A. van Uden, Ph.D. thesis, University Utrecht, 1997.
[4] J. M. Laget, Nucl. Phys. **A194**, 81 (1972).
[5] G. van der Steenhoven, in *Proceedings of the 4th Workshop on Perspectives in Nuclear Physics at Intermediate Energies*, Trieste, 1989, edited by S. Boffi, C. Ciofi delgi Atti, and M. Giannini (World Scientific, Singapore, 1989), p. 469.
[6] K. I. Blomqvist and J. M. Laget, Nucl. Phys. **A280**, 405 (1977).
[7] J. M. Laget, Nucl. Phys. **A481**, 765 (1988).
[8] J. A. Carr, H. McManus, and K. Stricker, Phys. Rev. C **25**, 952 (1982).
[9] P. Schwandt *et al.*, Phys. Rev. C **26**, 55 (1982).
[10] M. Leuschner *et al.*, Phys. Rev. C **49**, 955 (1994).
[11] J. H. Koch, E. J. Moniz, and N. Ohtsuka, Ann. Phys. (N.Y.) **154**, 99 (1984).
[12] T. Sato and T. Takaki, Nucl. Phys. **A562**, 673 (1993).
[13] P. S. Anan'in and I. V. Glavanakov, Sov. J. Nucl. Phys. **52**, 205 (1990).
[14] L. D. Pham *et al.*, Phys. Rev. C **46**, 621 (1992).
[15] P. K. A. de Witt Huberts, Nucl. Phys. **A553**, 845c (1993).
[16] L. Tiator and L. E. Wright, Nucl. Phys. **A379**, 407 (1982).
[17] L. B. Weinstein *et al.*, Phys. Rev. C **47**, 225 (1993).
[18] C. de Vries *et al.*, Nucl. Instrum. Methods Phys. Res. A **223**, 1 (1984).
[19] F. Garibaldi *et al.*, Nucl. Instrum. Methods Phys. Res. A **314**, 1 (1992).
[20] L. Lapikás, Nucl. Phys. **A553**, 297c (1993).
[21] H. Müther and W. H. Dickhoff, Phys. Rev. C **49**, R17 (1994).
[22] J. A. MacKenzie, Ph.D. thesis, University of Edinburgh, 1995.